Optics Letters

High-resolution chalcogenide fiber bundles for infrared imaging

Bin Zhang,[1] Chengcheng Zhai,[1] Sisheng Qi,[1] Wei Guo,[1] Zhiyong Yang,[1,*] Anping Yang,[1] Xin Gai,[2] Yi Yu,[2] Rongping Wang,[2] Dingyuan Tang,[1] Guangming Tao,[3] and Barry Luther-Davies[2]

[1]Jiangsu Key Laboratory of Advanced Laser Materials and Devices, School of Physics and Electronic Engineering, Jiangsu Normal University, Xuzhou, Jiangsu 221116, China
[2]Centre for Ultrahigh-bandwidth Devices for Optical Systems (CUDOS), Laser Physics Center, Research School of Physics and Engineering, Australian National University, Canberra, ACT 2600, Australia
[3]CREOL, The College of Optics & Photonics, University of Central Florida, Orlando, Florida 32816, USA
*Corresponding author: yangzhiyong@jsnu.edu.cn

Received 8 July 2015; revised 4 August 2015; accepted 28 August 2015; posted 31 August 2015 (Doc. ID 245567); published 17 September 2015

An ordered chalcogenide fiber bundle with a high resolution for infrared imaging was fabricated using a stack-and-draw approach. The fiber bundle consisted of about 810,000 single fibers with an As_2S_3 glass core of 9 μm in diameter and a polyetherimide (PEI) polymer cladding of 10 μm in diameter. The As_2S_3/PEI fibers showed good transparency in the 1.5–6.5 μm spectral region. It presented a resolution of ~45 lp/mm and a crosstalk of ~2.5%. Fine thermal images of a hot soldering iron tip were delivered through the fiber bundle. © 2015 Optical Society of America

OCIS codes: (060.2280) Fiber design and fabrication; (060.2390) Fiber optics, infrared; (060.2350) Fiber optics imaging; (110.3080) Infrared imaging.

http://dx.doi.org/10.1364/OL.40.004384

Infrared imaging systems have been widely used in many fields such as medicine, industry, and defense [1–3]. In extreme (e.g., under nuclear irradiation) or unfavorable environments (e.g., stray electromagnetic fields, in restricted spaces, etc.), the use of a flexible, ordered fiber bundle (FB) for collection and delivery of infrared images is desirable. While state-of-the-art oxide glass FBs [4] have been manufactured and used to transmit high-resolution images in the visible and near-infrared spectral regions, they are opaque at wavelengths longer than about 2.5 μm because of the intrinsic multi-phonon absorptions of the oxide glasses. Currently, FBs capable of transmitting infrared images are mainly based on chalcogenide glass fibers [5–8], silver halide crystalline fibers [9–11], and hollow capillary (HC) fibers [12–14]. Chalcogenide glass fibers show good transmittance in the 1–7 μm (sulfide), 2–9 μm (selenide), and 3–12 μm (telluride) spectral ranges, depending on their compositions. Through the conventional "layer winding method" [7], chalcogenide FBs with good flexibility can be fabricated. However, the resulting FBs typically have a low resolution because it is difficult to reduce the diameter of individual fibers to less than 40 μm [15]. Silver halide fibers have good transparency in the 4–20 μm spectral range. Using a multiple-extrusion approach, FBs consisting of 9000 AgClBr single fibers with a diameter as small as 25 μm have been fabricated [16]. HC fibers can transmit light in the 3–14 μm region. An HC FB can be produced by first fabricating an FB consisting of single HC fibers, and then coating metal and dielectric films (e.g., Ag/AgI) on the inner surfaces of the hollow capillaries [12]. However, it is challenging to fabricate a long HC FB due to the restriction of the coating process. The HC fibers in the FB also exhibit losses as high as tens of dB/m.

The infrared FBs reported to date typically have resolutions of less than 10 lp/mm, and therefore can only transmit relatively coarse infrared images. In this Letter, we fabricated an ordered chalcogenide FB with a resolution as high as 45 lp/mm. The FB contained about 810,000 single fibers with an As_2S_3 glass core of 9 μm in diameter and a polyetherimide (PEI) polymer cladding of 10 μm in diameter. Its optical properties were characterized, and its ability to deliver an infrared image was verified.

The fabrication process of the As_2S_3/PEI FB is depicted in Fig. 1. In the first step, a fiber with a diameter of 400 μm was thermally drawn from a 100 mm-long cylindrical preform consisting of an As_2S_3 glass core with a diameter of 18 mm and a PEI cladding with a diameter of 20 mm [Fig. 1(a)]. In the second step, the fiber was cut into segments of 200 mm in length, and about 900 segments were stacked to form a hexagonal column with a side length of 6.5 mm. Then, the hexagonal column was rolled with PEI films to form a preform with a side length of 7.8 mm, which was then thermally drawn into a "multi-fiber" with a side length of 200 μm [Fig. 1(b)]. In the third step, the multi-fiber was cut into segments that were each 200 mm long, and about 900 segments were stacked again to form a hexagonal column with a side length of 6.5 mm, which was subsequently rolled with protective PEI films and thermally consolidated under a vacuum to form the final FB [Fig. 1(c)]. The obtained FB consisted of about 810,000 single fibers, and had a cross section of about 110 mm^2. The cross section of the FB is shown in Fig. 1(d), indicating that the core diameter

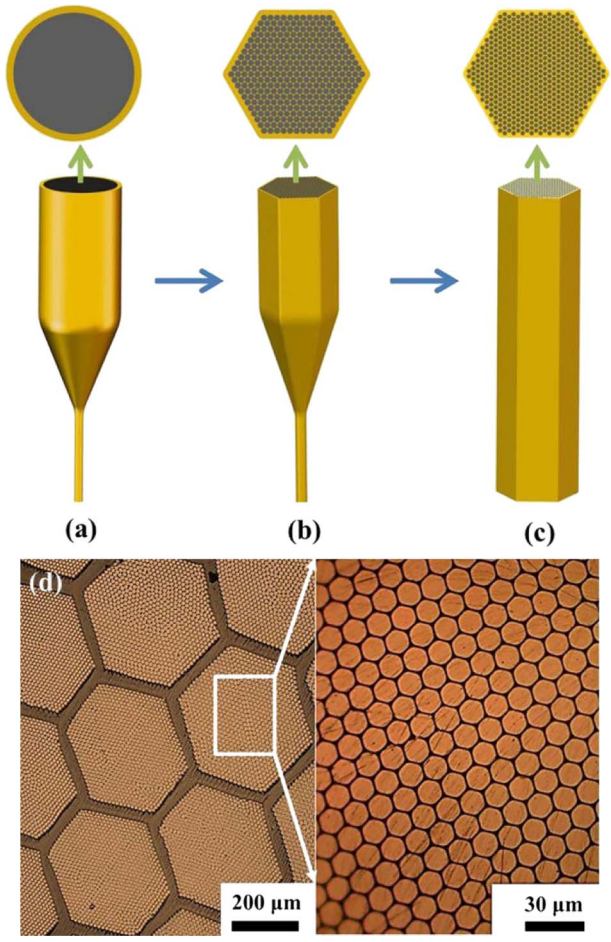

Fig. 1. Schematic of fabrication process for the FB by a stack-and-draw technique. (a) Drawing of single fibers. (b) Stacking of single fibers and drawing of multi-fibers. (c) Stacking of multi-fibers and forming of the FB. (d) Cross sections of the fabricated FB consisting of 810,000 single fibers.

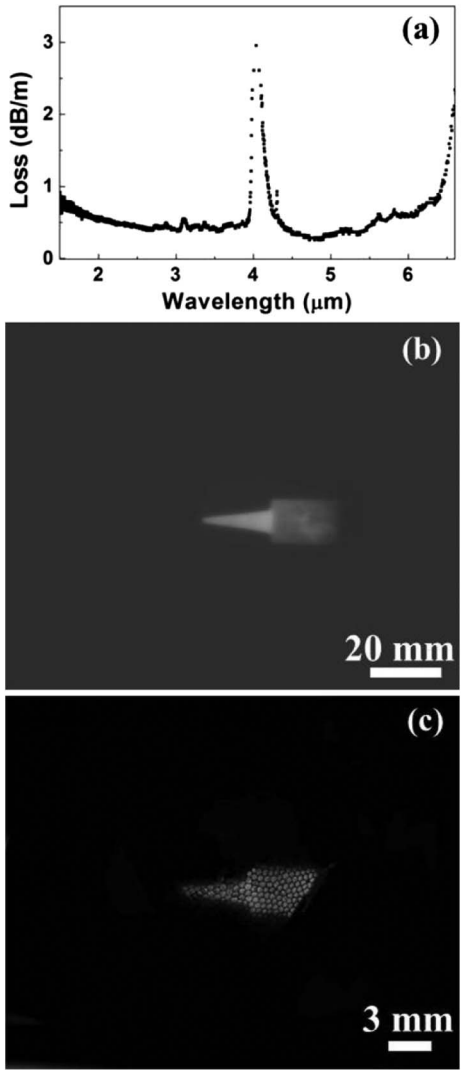

Fig. 2. (a) Attenuation of fabricated As_2S_3/PEI fibers with a core diameter of 360 μm and a cladding diameter of 400 μm. (b) Infrared images of a soldering iron tip taken with an InSb camera directly and (c) captured through a 50 mm-long As_2S_3/PEI FB.

was about 9 μm and the pitch between the cores was about 10 μm. The active area (or filling factor) of the FB, which was defined by the percentage of the core area in the cross section, was about 50%. This value could be increased significantly by reducing the thickness of the PEI gaps between the multi-fibers.

In the fabrication of the high-resolution FB, PEI was intentionally chosen as the cladding material because of its several advantages: (1) it is a thermoplastic polymer with a high glass transition temperature of ~215°C, and therefore is thermally compatible with quite a few chalcogenide glasses, such as As_2S_3 and As_2Se_3 [17,18]. The spatial arrangement of stacked fibers can be easily preserved during the drawing process. This makes it feasible to produce high-resolution FBs through a stack-and-draw approach. (2) PEI has high strength [19]. It protects the fragile As_2S_3 glass core during the whole fabrication process, and therefore helps to reduce the possibility of forming dark (broken) fibers in the FB. (3) It has high rigidity. A PEI polymer and As_2S_3 glass can be well polished together [Fig. 1(d)]. This makes it convenient to obtain an FB with shaped ends by post-mechanical processing. (4) Compared to As_2S_3 core glass with a refractive index (RI) of ~2.4, PEI has a much lower RI of ~1.65. This creates a large RI contrast between the core and cladding, leading to a very high numerical aperture [5] (NA of ~1.74) fiber with excellent light confinement ability.

High-purity glass is crucial for fabricating low-loss fibers and therefore high-performance FBs for infrared imaging. The As_2S_3 glass was synthesized from 6N-purity elemental arsenic and sulfur using the conventional melt-quenching technique [20]. To improve the purity of the glass, physical and chemical distillation techniques [21,22] were applied in the synthesis. The transmission losses of the fabricated As_2S_3/PEI fibers were measured by the cut-off method using a Bruker tensor 27 Fourier transform infrared spectrophotometer (FTIR) equipped with an external fiber coupling accessory and an HgCdTe detector cooled with liquid nitrogen. The fiber with a core diameter of 360 μm and a cladding diameter of 400 μm, which was drawn in the first step, had good transmission in the 1.5–6.5 μm region [Fig. 2(a)]. The background loss was about 0.5 dB/m, and the loss at 4.0 μm, which corresponded to the absorption band

due to S-H impurities, was about 3 dB/m. The individual fibers in the FB could have higher losses, but our FTIR system was not able to measure them because of the very small core size.

The performance of the FB for transmitting infrared images was tested with a homemade imaging setup. A soldering iron tip with a temperature of 380°C was imaged on the input end of the FB using a CaF_2 lens. Another CaF_2 lens was then used to collect the transmitted signal from the output end of the FB and image it onto a Xenics InSb camera, which is sensitive from 1 to 5 μm in the mid-infrared. Figures 2(b) and 2(c) show the infrared images obtained with the camera directly and captured through a 50 mm-long FB, respectively. The latter shows quite clearly the fine features of the soldering iron tip as indicated in the former without any distortions, implying the good performance of the FB for the delivery of infrared images.

The resolution of the FB was determined by measuring the modulation transfer function (MTF), which can be obtained using the knife-edge method [11,13]. A knife edge was illuminated with 3.8 μm of light generated by an optical parametric amplifier (OPA), and its image was formed on the input end of the FB. The image was transmitted to the output end of the FB and was recorded with the InSb camera. A gray-level line profile was digitally sampled perpendicular to the knife-edge direction, and the result provided the edge-spread function (ESF), which is shown in the insert of Fig. 3(a). The next step for calculating the MTF was to make some standard algebraic operations, including fitting the ESF with a Fermi function, differentiating the fitted ESF, conducting a Fourier transform of the differentiated function, and normalizing its magnitude to unity at zero frequency [23]. Figure 3(a) shows the derived MTF curve. The resolution of the bundle defined by the points where the intensity of the MTF was reduced to half of its maximum value was 45 lp/mm.

Crosstalk [8,11] may be observed in FBs when light focused into an individual fiber leaks into the near-neighbor fibers and is transmitted by those surrounding fibers. The crosstalk is the ratio between the total light intensity in the surrounding fibers ΣP_i to the intensity in the core of the exited fiber P_0:

$$C = \frac{\sum P_i}{\sum P_i + P_0}. \quad (1)$$

In the experiment, 3.8 μm of light generated by the OPA was coupled into a single fiber in a 50 mm-long FB using an NA = 0.57 diamond-turned ZnSe lens with an anti-reflection coating for the 3–5 μm band [24]. The focused spot size was estimated to be ~4 μm. The output from the FB was collected by a ×36 reflective objective lens and imaged onto the InSb camera. The image of the output is shown in Fig. 3(b). Using Eq. (1), about 2.5% crosstalk was obtained.

The good performance of the FB for infrared image delivery benefits from the high resolution and the low crosstalk. The high resolution results from the small diameter of the As_2S_3/PEI individual fibers and the large active area of the FB, and the low crosstalk is mainly attributed to the large NA of the fibers. We found that an As_2S_3/PEI FB, which contained fewer multi-fiber units and had a cross section of less than ~1 mm^2, showed relatively good flexibility. However, the flexibility was quite limited when the cross section of the FB was increased. In that case, good flexibility could be restored by wax-sealing both ends of the FB and dissolving the exposed PEI in solvents such as dimethylacetamide (DMAC) and dichloromethane (see Fig. 4). It should be noted that the fibers lost their cladding after the PEI was dissolved by the solvents. In that case, the crosstalk between the adjacent fibers was expected to get much higher and the FB was no longer suitable for transmitting infrared images. However, this gives an indication that it is feasible to achieve a useful infrared FB with a large cross section and high flexibility by employing a more complex fiber structure with a chalcogenide core, a chalcogenide inner cladding, and a PEI outer cladding, where the removal of the PEI by solvents should not disrupt the infrared guidance. In that case, the chalcogenide core has a chalcogenide cladding with a lower refractive index, and the PEI acts as an interlayer material similar to the "acid-dissolved glass" used in the manufacturing of the high-resolution oxide glass FBs [25].

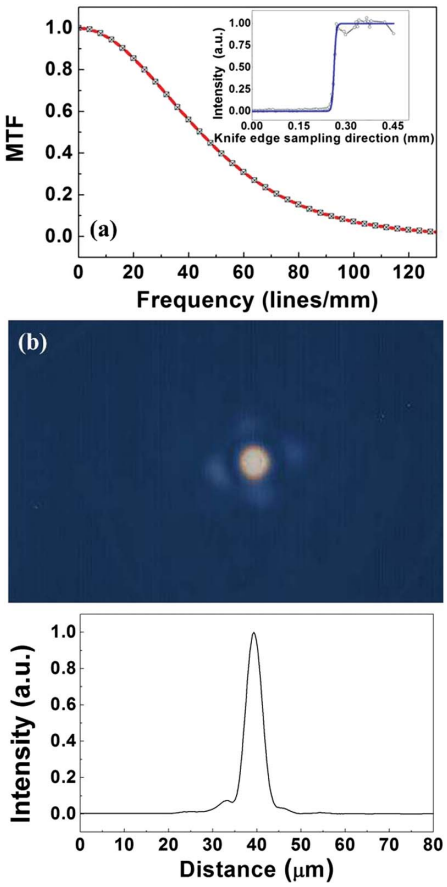

Fig. 3. (a) MTF of fabricated As_2S_3/PEI FB obtained by the knife-edge method. The inset image is the evolution of the total output intensity during the knife-edge measurement. (b) Light intensity distribution on the output end of fabricated As_2S_3/PEI FB in a crosstalk measurement.

In conclusion, we fabricated an ordered FB consisting of 810,000 single fibers with an As_2S_3 glass core of 9 μm in diameter and a PEI polymer cladding of 10 μm in diameter. The fiber showed good transparency in the 1.5–6.5 μm spectral region. The FB had a cross section of ~110 mm^2 and an active area of ~50%. It showed a high resolution of 45 lp/mm and a low crosstalk of ~2.5%, making it capable of transmitting thermal images of hot objects efficiently.

Fig. 4. Image of a FB consisting of 810,000 As_2S_3/PEI fibers after the PEI was dissolved by the DMAC solvent. The FB had a cross section of ~10 mm^2, which was obtained by further reducing the side length of the FB shown in Fig. 1(c) through the drawing process. The FB was put into a cup of water to show its flexibility more clearly.

Funding. National Natural Science Foundation of China (NSFC) (51303072, 61205207, 61405080); Natural Science Foundation of Colleges and Universities in Jiangsu Province (13KJB430013); Priority Academic Program Development of Jiangsu Higher Education Institutions; Jiangsu Collaborative Innovation Centre of Advanced Laser Technology and Emerging Industry.

REFERENCES

1. A. Rogalski and K. Chrzanowski, Opto-Electron. Rev. **10**, 111 (2002).
2. H. Golnabi and A. Asadpour, Rob. Comput. Integr. Manuf. **23**, 630 (2007).
3. B. B. Lahiri, S. Bagavathiappan, T. Jayakumar, and J. Philip, Infrared Phys. Technol. **55**, 221 (2012).
4. Y. Wenku, Y. Yuijing, Y. Tao, and D. Wenrong, Proc. SPIE **3242**, 284 (1997).
5. M. Saito, M. Takizawa, S. Sakuragi, and F. Tanei, Appl. Opt. **24**, 2304 (1985).
6. M. R. Paul Klocek and R. D. Rock, Opt. Eng. **26**, 88 (1987).
7. A. R. Hilton, A. R. Hilton, J. McCord, W. S. Thompson, and R. A. LeBlanc, Proc. SPIE **5074**, 849 (2003).
8. S. B. Mobley, B. Shaw, D. Gibson, V. Nguyen, R. Gattass, J. Sanghera, and I. Aggarwal, Proc. SPIE **8015**, 801503 (2011).
9. I. Paiss and A. Katzir, Appl. Phys. Lett. **61**, 1384 (1992).
10. Y. Lavi, A. Millo, and A. Katzir, Appl. Phys. Lett. **87**, 241122 (2005).
11. Y. Lavi, A. Millo, and A. Katzir, Appl. Opt. **45**, 5808 (2006).
12. V. Gopal, J. A. Harrington, A. Goren, and I. Gannot, Opt. Eng. **43**, 1195 (2004).
13. U. Gal, J. Harrington, M. Ben-David, C. Bledt, N. Syzonenko, and I. Gannot, Appl. Opt. **49**, 4700 (2010).
14. C. H. Huang, S. Kino, T. Katagiri, and Y. Matsuura, Appl. Opt. **51**, 6913 (2012).
15. A. R. Hilton, A. R. Hilton, J. McCord, and W. S. Thompson, Proc. SPIE **4204**, 300 (2001).
16. E. Rave, L. Nagli, and A. Katzir, Opt. Lett. **25**, 1237 (2000).
17. J. J. Kaufman, G. Tao, S. Shabahang, E.-H. Banaei, D. S. Deng, X. Liang, S. G. Johnson, Y. Fink, and A. F. Abouraddy, Nature **487**, 463 (2012).
18. J. J. Kaufman, R. Ottman, G. Tao, S. Shabahang, E.-H. Banaei, X. Liang, S. G. Johnson, Y. Fink, R. Chakrabarti, and A. F. Abouraddy, Proc. Natl. Acad. Sci. USA **110**, 15549 (2013).
19. G. Tao, S. Shabahang, H. Ren, F. Khalilzadeh-Rezaie, R. E. Peale, Z. Yang, X. Wang, and A. F. Abouraddy, Opt. Lett. **39**, 4009 (2014).
20. M. F. Churbanov, V. S. Shiryaev, A. I. Suchkov, A. A. Pushkin, V. V. Gerasimenko, R. M. Shaposhnikov, E. M. Dianov, V. G. Plotnichenko, V. V. Koltashev, Y. N. Pyrkov, J. Lucas, and J. L. Adam, Inorg. Mater. **43**, 441 (2007).
21. M. F. Churbanov, G. E. Snopatin, V. S. Shiryaev, V. G. Plotnichenko, and E. M. Dianov, J. Non-Cryst. Solids **357**, 2352 (2011).
22. B. Zhang, W. Guo, Y. Yu, C. C. Zhai, S. S. Qi, A. P. Yang, L. Li, Z. Y. Yang, R. P. Wang, D. Y. Tang, G. M. Tao, and B. Luther-Davies, J. Am. Ceram. Soc. **98**, 1389 (2015).
23. E. Rave, D. Shemesh, and A. Katzir, Appl. Phys. Lett. **76**, 1795 (2000).
24. Y. Yu, X. Gai, P. Ma, D. Y. Choi, Z. Y. Yang, R. P. Wang, S. Debbarma, S. J. Madden, and B. Luther-Davies, Laser Photon. Rev. **8**, 792 (2014).
25. J. Hecht, *Understanding Fiber Optics*, 5th ed. (Prentice-Hall, 2005), p. 1.

130.56.97.170 {ts '2016-10-05 17:57:24'}